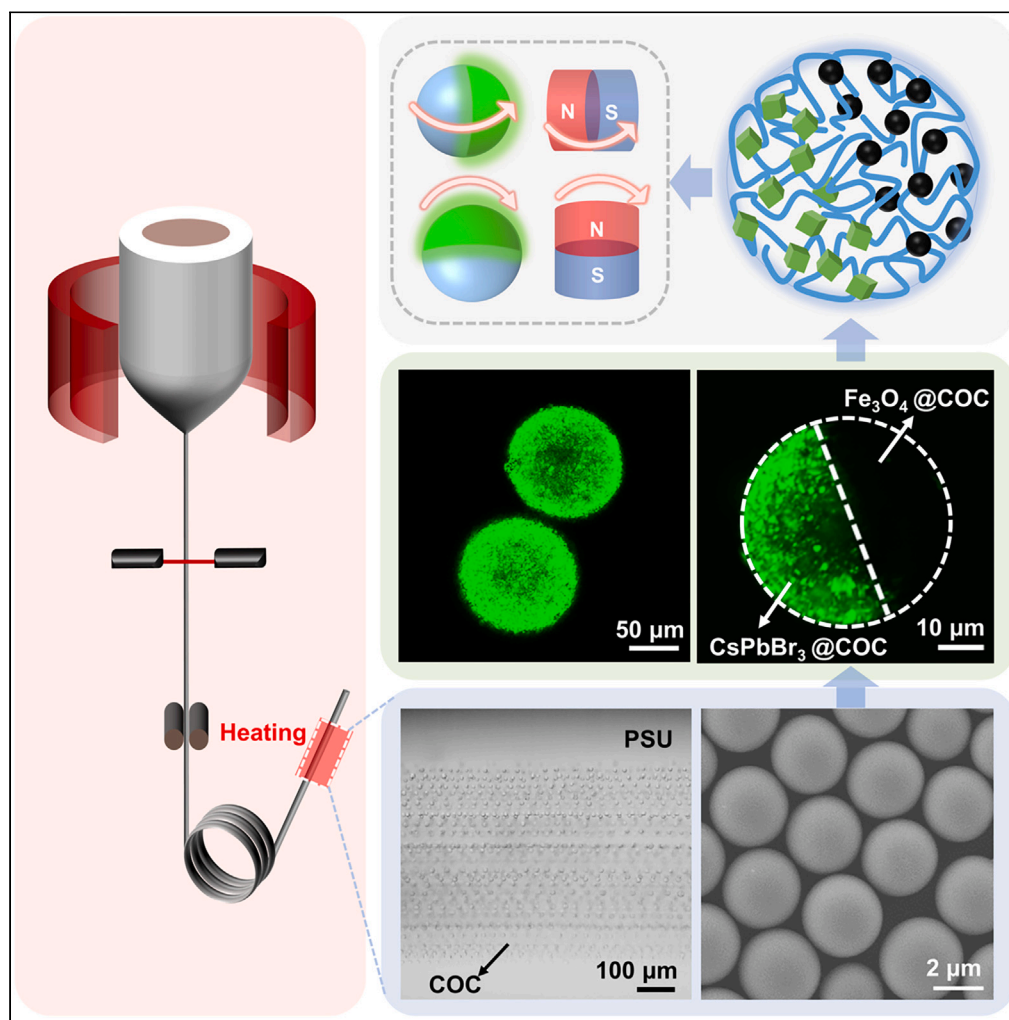**Article**

Development of structure-tailored and composite magnetic-fluorescent microspheres through the PRI method

Haochuan Yang,
Khalid Javed, Xi Li,
..., Haiping He,
Xvsheng Qiao,
Guangming Tao

qiaoxus@zju.edu.cn (X.Q.)
tao@hust.edu.cn (G.T.)

Highlights

Employed Plateau-Rayleigh capillary instability for 500nm–500μm polymer microspheres

Integration of CsPbBr$_3$ QDs and Fe$_3$O$_4$ NCs for magnetic-fluorescent Janus microspheres

Precise remote luminescence control in Janus microspheres under external magnetic field

Article

Development of structure-tailored and composite magnetic-fluorescent microspheres through the PRI method

Haochuan Yang,[1,7] Khalid Javed,[1,2,7] Xi Li,[1] Yuqi Zou,[2] Xingliang Dai,[3] Haiping He,[3] Xvsheng Qiao,[1,8,*] and Guangming Tao[2,4,5,6,*]

SUMMARY

Multifunctional micro- and nanoparticles have found their applications in fields like medicine, display materials, cosmetics, and so on. Advances in these fields have been demonstrated to need scalable uniformly sized, mass-produced, and structured spherical particles. In this work, we proposed structure-tailored and multifunctional composite polymeric microspheres with tunable diameter size, by using a versatile and scalable in-fiber particle fabrication through the Plateau-Rayleigh capillary instability method. The results show that the characteristic shapes of the luminescence spectra of $CsPbBr_3$ remained similar before and after embedding in the microspheres. The luminescence intensity was stabilized at 85–90% of their original photoluminescence intensities over an extended period. Moreover, the photoluminescence lifetime of the fluorescent microspheres was increased by 9.03% compared to $CsPbBr_3$. The X-ray diffraction results revealed that there was no change in the crystal structure of the dopants before and after the encapsulation. Also, precise magnetic manipulation of Janus microspheres was successfully demonstrated.

INTRODUCTION

Multifunctional microspheres have several applications including medicine,[1] anti-counterfeiting,[2,3] remote manipulation, and displays.[4–6] In most of the applications, the fluorescence and magnetization functions have been used more frequently. One type of multifunctional microspheres called Janus is a single particle having two regions with different properties.[7] Recently, Janus microspheres have gotten great attention because of their asymmetric nature. The ability to integrate tailorable multifunctions in single particle has made them a smart building block for designing the next generation intelligent materials.[8] Several methods including microfluidic technique, surface modification, electrified co-jetting, and spinning disks technique have been utilized to fabricate Janus particles with different shapes, functionalities, and nature.[9–11] For example, Li et al.[12] reported the fabrication of fluorescent-magnetic Janus microspheres by electrospraying. Chen et al.[13] reported the fabrication of magnetic Janus photonic crystal microbeads with multiple fluorescence colors by microfluidic method. Yin et al.[10] demonstrated the Janus microspheres fabrication with magnetic-fluorescent parts via the microfluidic device. According to literature,[14,15] particles' application mostly depends on fabrication method and particle size. But, most of these wet methods used to prepare Janus particles have issues like large particle size dispersion,[16] and low yield which prevent the wide use of these methods.[17] So, a reliable and easy-to-use method to fabricate Janus particles with good control of shape, size, composition, and scalability is still considered a major challenge.

To address the challenges mentioned above, a physical top-down in fiber "Plateau-Rayleigh capillary instability (PRI)" method, which has several advantages over conventional wet methods, was proposed recently. By using this method, the fabricated particles have a clean surface, high yield as well as Janus structure with a diameter ranging from 100 μm down to 3 μm by optimizing parameters like temperature, preform feed speed, and fiber draw speed. Shabahang and A. F. Abouraddy et al., (2011) reported the first observation of PRI at the core-cladding interface in multimaterial fiber.[18] Later, Kaufman and Tao et al., (2012) have shown the ability of this in-fiber PRI method to fabricate the structured particles with uniform size by thermally drawing the multimaterial fibers.[16] Also, Tao et al., (2016) presented a scalable fabrication approach for digital designing the internal geometry of multimaterial photonic particles.[19] For magnetic-fluorescent Janus

[1]School of Materials Science and Engineering, Zhejiang University, Hangzhou, Zhejiang 310027, China
[2]Wuhan National Laboratory for Optoelectronics, Huazhong University of Science and Technology, Wuhan, Hubei 430074, China
[3]School of Materials Science and Engineering, State Key Laboratory of Silicon Materials, Zhejiang University, Hangzhou, Zhejiang 310027, China
[4]Key Laboratory of Vascular Aging, Ministry of Education, Tongji Hospital Tongji Medical College, Huazhong University of Science and Technology, Wuhan, Hubei 430030, China
[5]State Key Laboratory of Material Processing and Die & Mould Technology, School of Materials Science and Engineering, Huazhong University of Science and Technology, Wuhan, Hubei 430074, China
[6]School of Physical Education, Huazhong University of Science and Technology, Wuhan, Hubei 430074, China
[7]These authors contributed equally
[8]Lead contact
*Correspondence: qiaoxus@zju.edu.cn (X.Q.), tao@hust.edu.cn (G.T.)
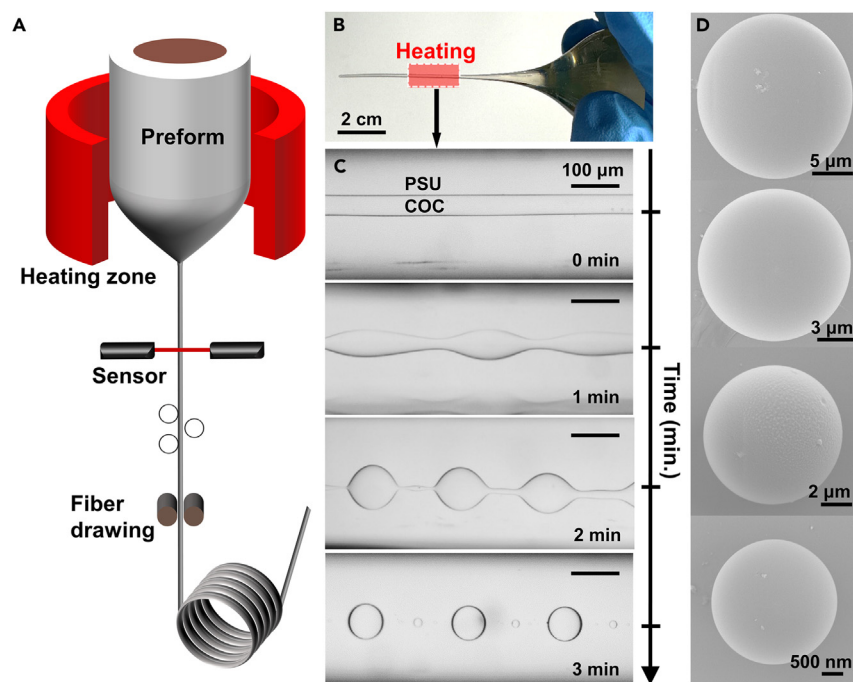https://doi.org/10.1016/j.isci.2024.110407

Figure 1. In-fiber polymer microspheres fabrication through PRI method

(A) Schematic of the preform-to-fiber thermal drawing process through a fiber drawing tower.

(B) A preform (d ~25 mm) has been thermally drawn into a fiber.

(C) Optical side view of the fiber during heat treatment at 380°C from 0 to 3 min.

(D) COC microspheres' (d ~ 3 to 30 μm) SEM images.

microspheres fabricated by the in-fiber PRI method, we doped superparamagnetic Fe_3O_4 in one semi-sphere to get magnetic functionality, whereas for the other semi-sphere the $CsPbBr_3$ Perovskite quantum dots (PQDs) has been used for fluorescent functionality. Although most of the researchers have used fluorescent dye molecules to prepare composite fluorescence microspheres,[20,21] they have issues like unstable optical properties, narrow excitation, and wide emission wavelength.[22] To avoid these problems, we have selected $CsPbBr_3$ PQDs because they have exceptional photovoltaic and optoelectronic properties.[23–25] However, when exposed to light, heat or moister these PQDs show poor stability which limit their potential applications.[26–28] One way to overcome this issue is polymer encapsulation of these PQDs to make them more resistant against environmental factors.

In this work, structure-tailored and composite magnetic-fluorescent microspheres have been fabricated by using an efficient and versatile in-fiber PRI method.[29–31] Here we are reporting the synthesis of composite magnetic-fluorescent microspheres from 100 μm down to 3 μm. The microspheres have been developed under the influence of surface tension, so their surface was extremely smooth. We have used a stack-and-draw approach to put multiple cores in a single fiber to induce PRI simultaneously for mass production. It makes them highly suitable and potential candidates for many applications.

RESULTS AND DISCUSSION

We have used the in-fiber particle fabrication through the PRI method to prepare microspheres with tunable diameter as shown in Figure 1. In this method, a centimeter-scaled model called "preform" is heated at a specific temperature to get a viscous state, and then stretched to get fibers. Multimaterial fibers have been realized using this technique during the last several years.[32–36] The schematic of the preform-to-fiber drawing process is shown in Figure 1A, whereas Figure 1B illustrates a section of fiber formed by thermal drawing and a conical-shaped pre-form obtained after melting. During this process, the temperature of the furnace was set around the softening temperature of the cladding material to maintain the continuity of the fiber and the intrinsic dimensional proportionality between the core and cladding.[16] The fibers after getting out of the heating zone were rapidly cooled to room temperature to prevent any axial instability phenomena. Typical prefabricated rods are shown in Figure S1. SEM of the cross-section show that the fibers retain the same core/cladding structure as the preform, and the dimensional ratios are consistent (Figure S2).

The PRI was induced in the fiber by thermal treatment,[18] and the dynamics of heat treatment over time for breakup process has been shown in Figure 1C. At the low temperature the viscosity is large which keeps the core intact, but with the increase in temperature the viscosity decreased, and surface tension reduces the inertial viscous forces causing the instability growth until cylindrical fluid converted into droplets. A sinusoidal modulation emerges at the interface and the depth of this modulation continue to increase until the core converted into droplets.

The "mother" droplets were connected by a bridge until they detached and left small "satellite" microspheres in the middle.[18,37] These microspheres remain steady in the cladding after cooling down to room temperature. The N, N-dimethylacetamide solution (DMAC) has been used to dissolve the PSU, to release these microspheres.

This in-fiber PRI approach has several key benefits. First, the spherical microspheres with uniform and tunable diameters as well as with a wide diameter range can be prepared. Second, it has ability for mass production/scalability. A large number of microspheres can be fabricated by using stack-and-draw method, in which several cores in the same fiber breakup simultaneously. Third, the ability of this approach to fabricate microspheres with complex structures (core-shell, Janus, and beach ball) by designing and preparing the macroscopic preform with the required structure. The fluid instability theory describes that when a cylindrical fluid is encased in another fluid, a sinusoidal wave (wavelength: λ) will emerge at the liquid surface because of difference in materials' surface tensions, as shown in Figure 1C. The PRI process can be explained by the equation given below:

$$\Delta P = \gamma \left(\frac{1}{R_1} + \frac{1}{R_2} \right) \qquad \text{(Equation 1)}$$

here R_1, and R_2 are the radius of curvature, surface tension coefficient is represented by γ, and ΔP describes the pressure difference. From two factors we can determine the diameter of spherical microspheres: (i) instabilities wavelength (λ) and (ii) rate of perturbations (τ). The perturbation rate "τ" can be calculated using the Tomotika's linear theory:[38,39]

$$\tau = D_0 \mu_{clad} / \left[\gamma_i \left(1 - \eta^2 \right) \Phi(\eta, \mu_{core} / \mu_{clad}) \right] \qquad \text{(Equation 2)}$$

where D_o is core diameter, μ is viscosity of the material, γ_i is interfacial surface tension, Φ is a defined function,[38] and $\eta = \frac{\pi D_0}{\lambda}$. When the heating time is greater than the τ, then capillary instability has enough time to shrink the steady fluid to break-up into spherical microspheres. By controlling the core diameter "D_o" we can tune the final particle diameter "D" as illustrated below:[40]

$$D = \sqrt[3]{3\pi/2\eta} \, D_o \qquad \text{(Equation 3)}$$

Considering excellent thermal stability and exceptional optical properties of the COC, it has been selected as core material in this work.[41] Also, after fiber drawing, we need to remove the cladding material using selective solvent. Thus cladding materials should have opposite dissolution properties as compared with core material to ensure that the dissolution will not cause any loss of the core material. Furthermore, in PRI approach the heat treatment requires that the softening temperature of the cladding material should be higher than that of the core material. Considering this, polysulfone (PSU) was selected as the cladding material.

After getting expertise in fiber drawing process,[42–47] we have analyzed and optimized different parameters like temperature, feed speed, and draw speed, to study their effect on the fiber diameter, which has linear relation with particle diameter (Equation 3). The particle size control was confirmed by SEM images of some selected samples shown in Figure 1D, with diameter range from ~30 μm to ~3 μm, highlighting the flexibility of the in-fiber PRI method in tuning particle size. This excellent tunability of diameter size from several millimeter to several nanometers is a key benefit of this approach which is difficult to realize by using the conventional wet methods. Also, we can control the particle size by optimizing the inner and outer diameters of preform.

The scalability of in-fiber particle fabrication through PRI using stack-and-draw approach was demonstrated as shown in Figure 2. We have integrated 200 COC rods in PSU cladding to create a preform, which was thermally drawn to get a fiber with 200 cores as shown in Figures 2A and 2B. Then, this fiber was used to obtain polymer microspheres with uniform size after heat treatment at 380°C to induce PRI as shown in Figure 2C.

SEM images have shown that the microspheres had clean surfaces and were not adherent to each other (Figures 2D and 2E). For particle size analysis, we used the previously reported method of calculating 100 microspheres in SEM images by the ImageJ software.[48] The size results of the distribution are shown in Figure 2F. It showed that the distribution was very narrow, with an average D ~3.15 ± 0.16 μm. This stack-and-draw approach significantly increased the yield of microspheres by several orders of magnitude. Additionally, the optical transmission microscopy images revealed that due to the barrier of the cladding material between the cores, despite the close proximity of the cores to each other (~20 μm), they remain in place after heat treatment in the form of regularly arranged three-dimensional arrays.

We have fabricated the fluorescent composite microspheres CsPbBr$_3$@COC through PRI approach as shown in Figure 3. The solution blending method was used to mix a 10% doping ratio of inorganic CsPbBr$_3$ with the COC matrix. After optimizing the parameters like composition, mixing time, and temperature, the enhanced doping effect has been achieved. The cores with fluorescence function (Figure S3) were integrated with the cladding to form the preform. Then the fiber drawing and particle processing were conducted similarly as has been done for undoped samples. The photograph of the fluorescent polymeric microspheres under ambient light and UV excitation, fabricated through PRI method, was shown in Figure S4.

The confocal laser scanning microscopy (CLSM) luminescence images of two representative microspheres (size ~100 μm) have been shown in Figures 3A and 3B, and the fluorescence results demonstrated that the CsPbBr$_3$ microspheres have been effectively encapsulated within the polymer microspheres. To explore the spatial distribution of CsPbBr$_3$ in the composite microspheres, we scanned a randomly selected fluorescent microsphere using the z stack mode of the CLSM. As shown in Figure 3C, the CsPbBr$_3$@COC displayed uniform and bright fluorescence in every randomly selected focal plane, indicating uniform dispersion of the fluorescent substance throughout the microspheres. Additionally, as revealed by the X-ray diffraction (XRD) results in Figure 3D, typical crystal diffraction peaks were observed alongside the amorphous structure corresponding to the polymer matrix, which closely match the structure of CsPbBr$_3$ (PDF No. 18–0364).
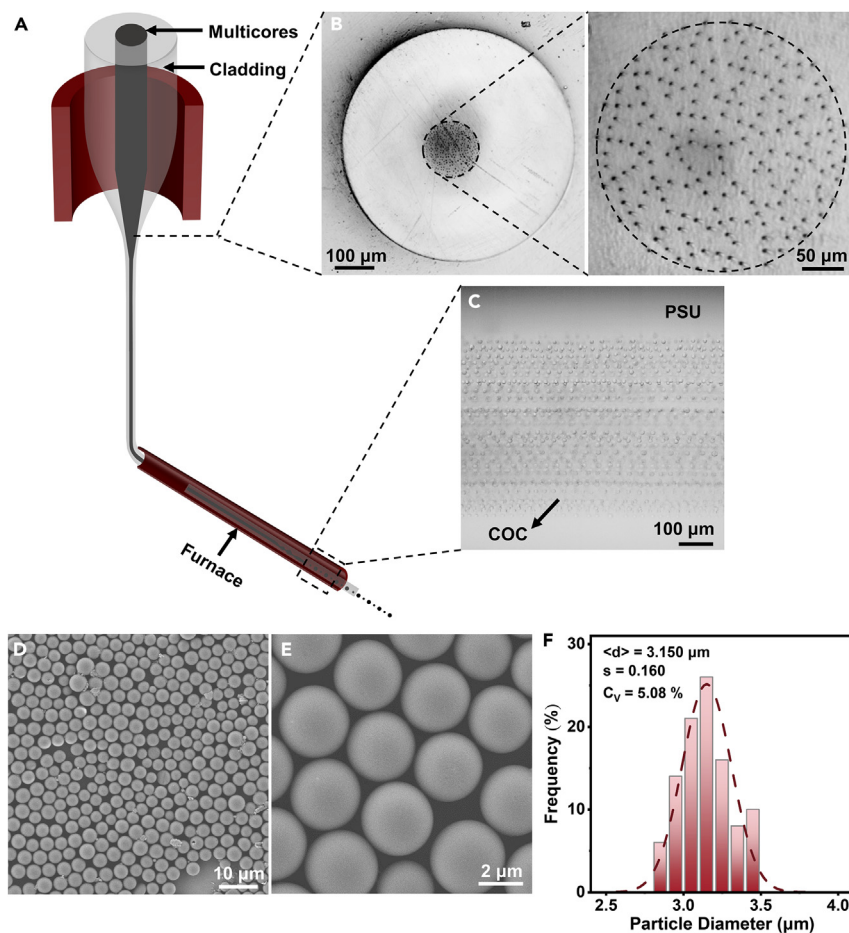
Figure 2. Scalable in-fiber polymer microspheres fabrication

(A) Schematic diagram of a multicore preform thermally drawn into fiber, then the cores were annealed to form spherical droplets and released from the cladding by selective dissolution.

(B) Optical image of fiber cross-section with 200 COC cores in the PSU cladding.

(C) Fiber side view optical transmission image after inducing PRI.

(D) SEM image of 3 μm (average diameter) COC microspheres in good number.

(E) Zoomed-in SEM image of some microspheres from (D) exhibiting clean and smooth surface.

(F) The size distribution of COC microspheres.

The optical properties of the fluorescent microspheres were also characterized. Figure 3E shows the normalized fluorescence excitation and emission spectra of CsPbBr$_3$@COC microspheres and CsPbBr$_3$. The results reveal that the characteristic shapes of the luminescence spectra of CsPbBr$_3$ remained similar before and after embedding in the microspheres. However, its photoluminescence (PL) peaks were blue shifted from 520 nm to 515 nm compared to the CsPbBr$_3$. This indicates that the size of the PQDs decreased after being doped into the COC.[49,50] To observe the stability of CsPbBr$_3$@COC microspheres' fluorescent property, PL intensity spectra has been recorded after every 24 h for seven days. Figure 3F displays that all emission peaks for the fluorescent microspheres were stabilized at 515 nm. The luminescence intensity had a decay phenomenon (~15%) in the first 1–2 days, and then the green samples were stabilized at 85–90% of their original PL intensities in the subsequent time.

Also, the UV-Vis spectra has been shown in Figure S5, CsPbBr$_3$ has a characteristic absorption peak at 515 nm while the pure COC microspheres have no prominent absorption peak. The combined effect of these two materials has produce an insignificant absorption peak at 515 nm for CsPbBr$_3$@ COC microspheres. The time-resolved PL spectra of CsPbBr$_3$ and CsPbBr$_3$@COC samples were fitted using a tri-exponential function.[51]

$$I_{(t)} = A_1 \exp\left(-\frac{t}{\tau_1}\right) + A_2 \exp\left(-\frac{t}{\tau_2}\right) + A_3 \exp\left(-\frac{t}{\tau_3}\right) \qquad \text{(Equation 4)}$$

where $I_{(t)}$ is the emission intensity that changes with time, τ_1, τ_2, τ_3 are the lifetimes of different decay processes, and A_1, A_2, A_3 are the coefficients at these lifetimes.[52]
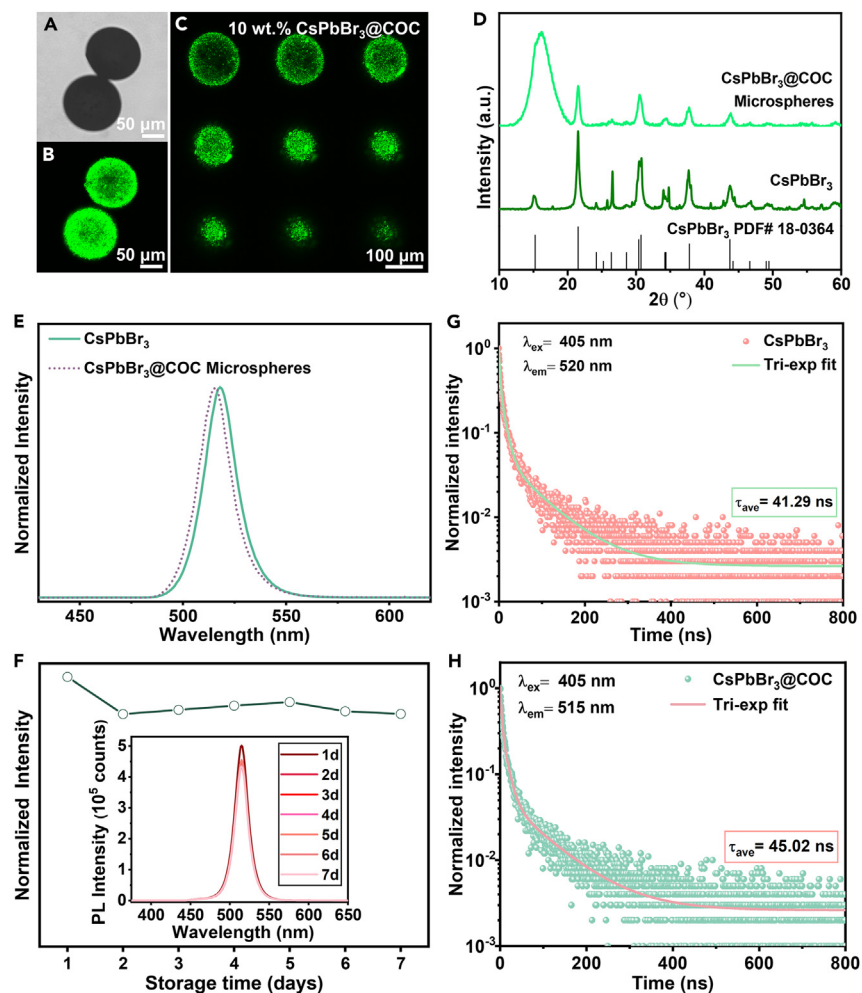
Figure 3. In-fiber fluorescent composite microspheres fabrication through PRI

(A and B) Bright-field and fluorescence images (excited by a 405 nm laser) of two fluorescent composite microspheres with diameters of about 100 μm.

(C) A series of CLSM luminescence images of sections of a microsphere, going from middle to bottom.

(D) XRD patterns of fluorescent composite microspheres.

(E) Fluorescence emission spectra of $CsPbBr_3$ and composite microspheres.

(F) PL intensity curves of the fluorescent microspheres dispersed in DMAC for a week.

(G and H) Decay curves and fitting results of $CsPbBr_3$ measured at 520 nm and composite microspheres measured at 515 nm.

$$\tau_{avg} = \frac{A_1\tau_1{}^2 + A_2\tau_2{}^2 + A_3\tau_3{}^2}{A_1\tau_1 + A_2\tau_2 + A_3\tau_3}$$

(Equation 5)

The results (Figures 3G and 3H) show that the average PL lifetime of $CsPbBr_3$ at 520 nm is 41.29 ns and that of the particles at 515 nm is 45.02 ns, which is an improvement of 9.03%. This means that non-radiative transitions are weakened and energy losses are reduced.[52] This may be because the surface of $CsPbBr_3$ is secondarily passivated by the flexible and dense COC polymer chains, which affects the radiative recombination of charge carriers and thus can effectively increase the fluorescence lifetime.

We have prepared the magnetic-fluorescent Janus microspheres by using this efficient and versatile in-fiber PRI method as illustrated in Figure 4. A magnetic-fluorescent composite COC cylindrical rod has been designed and fabricated. This rod has two-halves which were obtained by using a homemade customized mold. The one-half of the cylinder was doped with $CsPbBr_3$, while the other half was doped with Fe_3O_4 nanoparticles. Then this rod has been integrated with PSU cladding and thermally drawn to get the fiber. To obtain the magnetic-fluorescent Janus microspheres, the fiber drawing and particle processing were conducted in a similar way as has been done for undoped samples.

Fluorescent and magnetic functionalities of the Janus core was shown in Figures 4A, 4B and 4C. The photograph of the core rod has been shown in Figure 4A. The fluorescence properties of the half-cylindrical core containing $CsPbBr_3$ has been shown in Figure 4B, emitting bright
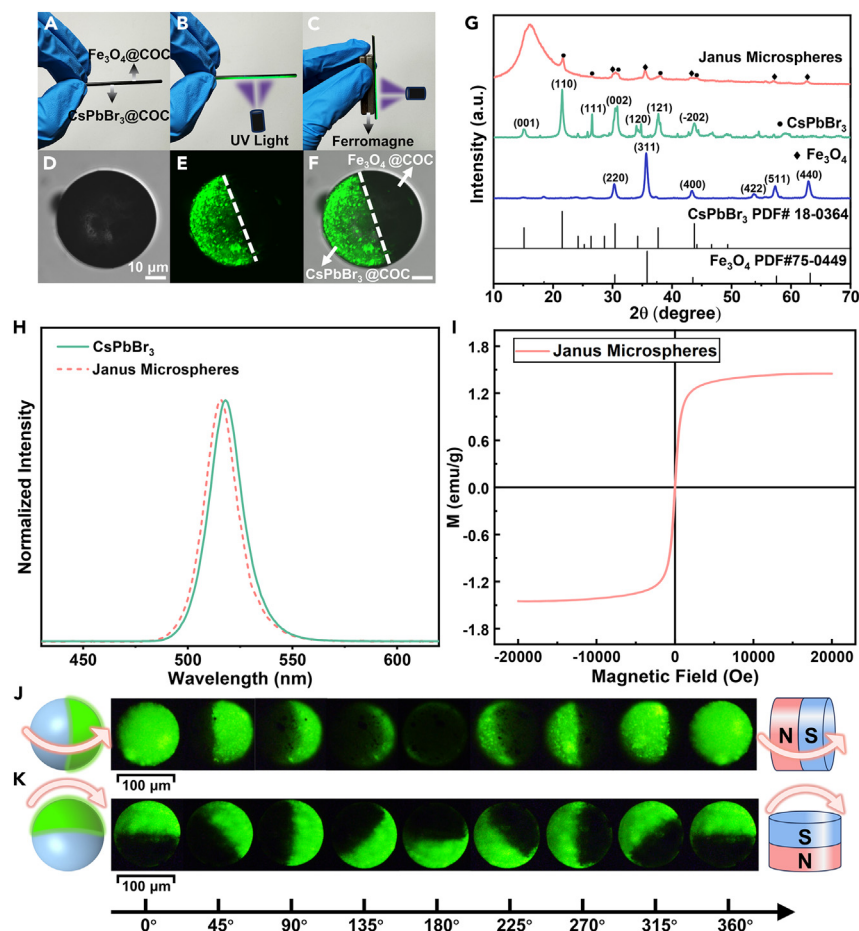
Figure 4. In-fiber fluorescent-magnetic Janus microspheres fabrication through PRI

(A–C) The Janus core of the preform processed through the customized mold, demonstrates dual functionality.

(D–F) CLSM luminescence images of the Janus particles, show clear hemispheric division.

(G) XRD patterns of Fe_3O_4, $CsPbBr_3$, and Janus particles.

(H) Fluorescence emission spectra of $CsPbBr_3$ and Janus particles.

(I) Hysteresis loop of Janus microspheres.

(J and K) Schematic and optical images showing the rotational motion of Janus particles under an external magnetic field.

green fluorescence under UV light, while the other half shows no response to UV light excitation. And the Figure 4C demonstrates the magnetic properties of the semi-cylindrical core containing Fe_3O_4 nanoparticles. It can be seen that the core rod is attracted in mid-air by an external magnetic field (generated by a ferromagnet). The CLSM was used to examine the distribution of the fluorescent material in the Janus microspheres. Figures 4D, 4E and 4F revealed that $CsPbBr_3$ is uniformly distributed on the fluorescent half of the microspheres. Whereas the other half containing Fe_3O_4 nanoparticles produced no fluorescence. Moreover, consistent with the earlier description, the images exhibit clear boundaries between the two hemispheres, mirroring the structure prior to the induction of PRI by heat treatment. This characteristic offers a novel approach for the future digital design of the multifunctional structured polymer microspheres. The XRD results for magnetic-fluorescent Janus microspheres (Figure 4G) proves that the composite particles were successfully prepared because the diffraction peaks of composite Janus particles coincide with those of Fe_3O_4 as well as $CsPbBr_3$, demonstrating that before and after the encapsulation there is no variation in the crystal structure of the dopants.

We have also investigated the optical properties of the magnetic-fluorescent Janus microspheres, the normalized fluorescence excitation and emission spectra of Janus microspheres and $CsPbBr_3$ were shown in Figure 4H. Similar to the fluorescent microspheres mentioned above, the PL emission peak of Janus microspheres undergoes a 5 nm blue-shift phenomenon. The Janus microspheres' magnetic properties were also characterized by using vibrating sample magnetometer (VSM). The results in Figure 4I show that the magnetic induction intensity of the microspheres is estimated to be ~1.5 emu g^{-1}, which makes them good candidate for potential applications like magnetic separation and display.

Remote manipulation of these Janus microspheres has been demonstrated and full dynamics were captured as shown in Figures 4J and 4K. The movement and orientation of the Janus microspheres can be manipulated by the external-magnetic field, thus making them useful for

fluorescent switching and displays. Given the superparamagnetic property of the doped iron oxide nanoparticles, we used two ferromagnets to manipulate Janus microspheres dispersed in DMAC and captured the dynamic process by the fluorescence microscope with a camera. It has been discovered that when the magnet is placed in such a way that its rotation axis is parallel to the substrate (Figure 4J), the rotation of the magnet causes the Janus particles to form multiple angles and ranges of the fluorescent face, and when the magnet is placed in such a way that its rotation axis is perpendicular to the substrate (Figure 4K), the Janus structured microspheres follow the magnet in the *in-situ* rotation.

Conclusions

In this work, a versatile, flexible, and scalable in-fiber microspheres fabrication through PRI method has been used to prepare undoped COC, $CsPbBr_3$ doped COC, and magnetic-fluorescent Janus ($CsPbBr_3//Fe_3O_4@COC$) microspheres with diameter size ranging from ∼100 μm down to ∼3 μm. By optimizing the temperature, preform feed-speed and fiber draw-speed, we have fabricated the microspheres with smooth surface and narrow size distribution (C_V < 5%). Also, the stack-and-draw approach enabled us to increase the microspheres' yield by several orders of magnitude by placing 200 fibers in preform core to induce the PRI simultaneously. The $CsPbBr_3@COC$ microspheres' fluorescence lifetime was enhanced by 9% and the fluorescence intensity remained stable around 90% of the initial intensity, whereas the Janus microspheres have demonstrated good response to external magnetic field for remote manipulation in both parallel and perpendicular directions of rotation. This work will be a key addition toward fabricating multifunctional polymeric particles with tunable size and complex structures.

Limitations of the study

Although the present work has played a significant role in the large-scale preparation of functional and/or complex structured microspheres, we found nonuniform doping of functional materials for microspheres with small diameter (∼3 μm). This is due to the fact that when doping has been done using the solution mixing method, the functional materials are agglomerated and thus their sizes are usually beyond the sub-micron range and some of the dopant material escapes from the substrate when the core breaks up. More efforts are needed to improve the doping for smaller diameter particles. One possible way is to use surface modification to enhance the binding capacity of the dopant to the matrix material.

STAR★METHODS

Detailed methods are provided in the online version of this paper and include the following:

- KEY RESOURCES TABLE
- RESOURCE AVAILABILITY
  - Lead contact
  - Materials availability
  - Data and code availability
- EXPERIMENTAL MODEL AND STUDY PARTICIPANT DETAILS
- METHOD DETAILS
  - COC/PSU preform fabrication
  - $CsPbBr_3$ preform fabrication with fluorescent function
  - Janus structured preform fabrication with fluorescent-magnetic multifunction
  - Fiber thermal drawing
  - Particles fabrication through the PRI method
  - Particle release
  - Characterization
- QUANTIFICATION AND STATISTICAL ANALYSIS

SUPPLEMENTAL INFORMATION

Supplemental information can be found online at https://doi.org/10.1016/j.isci.2024.110407.

AUTHOR CONTRIBUTIONS

H.Y. and K.J. investigated, designed, and conducted the experiments. H.Y. and X.L. fabricated the fibers and tested the particles. H.Y., K.J., X.L., Y.Z., X.D., H.H., X.Q., and G.T. wrote the manuscript with contributions from all authors. All authors discussed the results. X.Q. and G.T. supervised the research.

DECLARATION OF INTERESTS

The authors have no relevant financial interests in this article and no potential conflicts of interest to disclose.

REFERENCES

1. Daly, A.C., Riley, L., Segura, T., and Burdick, J.A. (2020). Hydrogel microparticles for biomedical applications. Nat. Rev. Mater. *5*, 20–43. https://doi.org/10.1038/s41578-019-0148-6.

2. Huanhuan, W., Shengyang, Y., Su-Na, Y., Li, C., and Su, C. (2015). Janus Suprabead Displays Derived from the Modified Photonic Crystals toward Temperature Magnetism and Optics Multiple Responses. ACS Appl. Mater. Interfaces *7*, 8827–8833. https://doi.org/10.1021/acsami.5b01436.

3. Zhang, H., Huang, C., Li, N., and Wei, J. (2021). Fabrication of multicolor Janus microbeads based on photonic crystals and upconversion nanoparticles. J. Colloid Interface Sci. *592*, 249–258. https://doi.org/10.1016/j.jcis.2021.02.068.

4. McConnell, M.D., Kraeutler, M.J., Yang, S., and Composto, R.J. (2010). Patchy and multiregion janus particles with tunable optical properties. Nano Lett. *10*, 603–609. https://doi.org/10.1021/nl903636r.

5. Glotzer, S.C. (2004). Materials science. Some Assembly Required. Science *306*, 419–420. https://doi.org/10.1126/science.1099988.

6. Howse, J.R., Jones, R.A., Ryan, A.J., Gough, T., Vafabakhsh, R., and Golestanian, R. (2007). Self-motile colloidal particles: from directed propulsion to random walk. Phys. Rev. Lett. *99*, 048102. https://doi.org/10.1103/physrevlett.99.048102.

7. Song, Y., and Chen, S. (2014). Janus nanoparticles: preparation, characterization, and applications. Chem. Asian J. *9*, 418–430. https://doi.org/10.1002/asia.201301398.

8. Yuan, Y., Wang, J., Xiang, Y., Zheng, S., Wu, Y., Liu, J., Zhu, X., and Zhang, Y. (2022). Shedding light on luminescent Janus nanoparticles: From synthesis to photoluminescence and applications. Small *18*, 2200020. https://doi.org/10.1002/smll.202200020.

9. Zhao, Q., Finlayson, C.E., Schaefer, C.G., Spahn, P., Gallei, M., Herrmann, L., Petukhov, A.V., and Baumberg, J.J. (2016). Nanoassembly of Polydisperse Photonic Crystals Based on Binary and Ternary Polymer Opal Alloys. Adv. Opt. Mater. *4*, 1494–1500. https://doi.org/10.1002/adom.201600328.

10. Yin, S.N., Wang, C.F., Yu, Z.Y., Wang, J., Liu, S.S., and Chen, S. (2011). Versatile bifunctional magnetic-fluorescent responsive janus supraballs towards the flexible bead display. Adv. Mater. *23*, 2915–2919. https://doi.org/10.1002/adma.201100203.

11. Meredith, C.H., Castonguay, A.C., Chiu, Y.-J., Brooks, A.M., Moerman, P.G., Torab, P., Wong, P.K., Sen, A., Velegol, D., and Zarzar, L.D. (2022). Chemical design of self-propelled Janus droplets. Matter *5*, 616–633. https://doi.org/10.1016/j.matt.2021.12.014.

12. Li, K., Li, P., Jia, Z., Qi, B., Xu, J., Kang, D., Liu, M., and Fan, Y. (2018). Enhanced fluorescent intensity of magnetic-fluorescent bifunctional PLGA microspheres based on Janus electrospraying for bioapplication. Sci. Rep. *8*, 17117. https://doi.org/10.1038/s41598-018-34856-z.

13. Chen, Y., Chen, Z., and Wei, J. (2023). Fe3O4 Nanoparticle-Based Janus Photonic Crystal Microbeads with Multiple Fluorescence Colors for Information Coding. ACS Appl. Nano Mater. *6*, 14702–14709. https://doi.org/10.1021/acsanm.3c02063.

14. Mahadik, B.P., Wheeler, T.D., Skertich, L.J., Kenis, P.J., and Harley, B.A. (2014). Microfluidic generation of gradient hydrogels to modulate hematopoietic stem cell culture environment. Adv. Healthcare Mater. *3*, 449–458. https://doi.org/10.1002/adhm.201300263.

15. He, C., Wei, X., Liang, T., Liu, M., Jiang, D., Zhuang, L., and Wang, P. (2021). Quantifying the compressive force of 3D cardiac tissues via calculating the volumetric deformation of built-in elastic gelatin microspheres. Adv. Healthcare Mater. *10*, 2001716. https://doi.org/10.1002/adhm.202001716.

16. Kaufman, J.J., Tao, G., Shabahang, S., Banaei, E.-H., Deng, D.S., Liang, X., Johnson, S.G., Fink, Y., and Abouraddy, A.F. (2012). Structured spheres generated by an in-fibre fluid instability. Nature *487*, 463–467. https://doi.org/10.1038/nature11215.

17. Nisisako, T., Torii, T., Takahashi, T., and Takizawa, Y. (2006). Synthesis of Monodisperse Bicolored Janus Particles with Electrical Anisotropy Using a Microfluidic Co-Flow System. Adv. Mater. *18*, 1152–1156. https://doi.org/10.1002/adma.200502431.

18. Shabahang, S., Kaufman, J., Deng, D., and Abouraddy, A. (2011). Observation of the Plateau-Rayleigh capillary instability in multi-material optical fibers. Appl. Phys. Lett. *99*, 161909. https://doi.org/10.1063/1.3653247.

19. Tao, G., Kaufman, J.J., Shabahang, S., Rezvani Naraghi, R., Sukhov, S.V., Joannopoulos, J.D., Fink, Y., Dogariu, A., and Abouraddy, A.F. (2016). Digital design of multimaterial photonic particles. Proc. Natl. Acad. Sci. USA *113*, 6839–6844. https://doi.org/10.1073/pnas.1601777113.

20. Yuet, K.P., Hwang, D.K., Haghgooie, R., and Doyle, P.S. (2010). Multifunctional superparamagnetic Janus particles. Langmuir *26*, 4281–4287. https://doi.org/10.1021/la903348s.

21. Lim, D.W., Hwang, S., Uzun, O., Stellacci, F., and Lahann, J. (2010). Compartmentalization of Gold Nanocrystals in Polymer Microparticles using Electrohydrodynamic Co-Jetting. Macromol. Rapid Commun. *31*, 176–182. https://doi.org/10.1002/marc.200900597.

22. Guan, Q., Song, R., Wu, W., Zhang, L., Jing, Y., Dai, H., and Fang, G. (2018). Fluorescent CdTe-QD-encoded nanocellulose microspheres by green spraying method. Cellulose *25*, 7017–7029. https://doi.org/10.1007/s10570-018-2065-z.

23. Chen, M., An, J., Hu, Y., Chen, R., Lyu, Y., Hu, N., Luo, Z., Yuan, M., and Liu, Y. (2020). Swelling-shrinking modified hyperstatic hydrophilic perovskite polymer fluorescent beads for Fe (III) detection. Sensor. Actuator. B Chem. *325*, 128809. https://doi.org/10.1016/j.snb.2020.128809.

24. Sanchez, S.L., Tang, Y., Hu, B., Yang, J., and Ahmadi, M. (2023). Understanding the ligand-assisted reprecipitation of CsPbBr3 nanocrystals via high-throughput robotic synthesis approach. Matter *6*, 2900–2918. https://doi.org/10.1016/j.matt.2023.05.023.

25. Peng, S., Wang, Y., Braun, M., Yin, Y., Meng, A.C., Tan, W., Saini, B., Severson, K., Marshall, A.F., Sytwu, K., et al. (2023). Kinetics and mechanism of light-induced phase separation in a mixed-halide perovskite. Matter *6*, 2052–2065. https://doi.org/10.1016/j.matt.2023.04.025.

26. Zhang, F., Zhong, H., Chen, C., Wu, X.-g., Hu, X., Huang, H., Han, J., Zou, B., and Dong, Y. (2015). Brightly luminescent and color-tunable colloidal CH3NH3PbX3 (X= Br, I, Cl) quantum dots: potential alternatives for display technology. ACS Nano *9*, 4533–4542. https://doi.org/10.1021/acsnano.5b01154.

27. Eperon, G.E., Habisreutinger, S.N., Leijtens, T., Bruijnaers, B.J., van Franeker, J.J., DeQuilettes, D.W., Pathak, S., Sutton, R.J., Grancini, G., Ginger, D.S., et al. (2015). The importance of moisture in hybrid lead halide perovskite thin film fabrication. ACS Nano *9*, 9380–9393. https://doi.org/10.1021/acsnano.5b03626.

28. Yang, S., Zhang, F., Tai, J., Li, Y., Yang, Y., Wang, H., Zhang, J., Xie, Z., Xu, B., Zhong, H., et al. (2018). A detour strategy for colloidally stable block-copolymer grafted MAPbBr 3 quantum dots in water with long photoluminescence lifetime. Nanoscale *10*, 5820–5826. https://doi.org/10.1039/C8NR01493K.

29. Gumennik, A., Wei, L., Lestoquoy, G., Stolyarov, A.M., Jia, X., Rekemeyer, P.H., Smith, M.J., Liang, X., Grena, B.J.B., Johnson, S.G., et al. (2013). Silicon-in-silica spheres via axial thermal gradient in-fibre capillary instabilities. Nat. Commun. *4*, 2216. https://doi.org/10.1038/ncomms3216.

30. Eggers, J., and Villermaux, E. (2008). Physics of liquid jets. Prog. Phys. *71*, 036601. https://doi.org/10.1088/0034-4885/71/3/036601.

31. Shabahang, S., Kaufman, J., and Abouraddy, A. (2011). Scalable fabrication of micro-and nano-particles utilizing the Rayleigh instability in multi-material fibers. Micro-and Nanotechnology Sensors, Systems, and Applications III *8031*, 758–764. https://doi.org/10.1117/12.883853.

32. Utada, A.S., Lorenceau, E., Link, D.R., Kaplan, P.D., Stone, H.A., and Weitz, D. (2005). Monodisperse double emulsions generated

from a microcapillary device. Science *308*, 537–541. https://doi.org/10.1126/science.1109164.

33. Yadavali, S., Jeong, H.-H., Lee, D., and Issadore, D. (2018). Silicon and glass very large scale microfluidic droplet integration for terascale generation of polymer microparticles. Nat. Commun. *9*, 1222. https://doi.org/10.1038/s41467-018-03515-2.

34. Day, R.W., Mankin, M.N., Gao, R., No, Y.-S., Kim, S.-K., Bell, D.C., Park, H.-G., and Lieber, C.M. (2015). Plateau–Rayleigh crystal growth of periodic shells on one-dimensional substrates. Nat. Nanotechnol. *10*, 345–352. https://doi.org/10.1038/nnano.2015.23.

35. Day, R.W., Mankin, M.N., and Lieber, C.M. (2016). Plateau–Rayleigh crystal growth of nanowire heterostructures: strain-modified surface chemistry and morphological control in one, two, and three dimensions. Nano Lett. *16*, 2830–2836. https://doi.org/10.1021/acs.nanolett.6b00629.

36. Tao, G., Stolyarov, A.M., and Abouraddy, A.F. (2012). Multimaterial fibers. Int. J. Appl. Glass Sci. *3*, 349–368. https://doi.org/10.1111/ijag.12007.

37. Xu, B., Ma, S., Xiang, Y., Zhang, J., Zhu, M., Wei, L., Tao, G., and Deng, D. (2020). In-fiber structured particles and filament arrays from the perspective of fluid instabilities. Adv. Fiber Mater. *2*, 1–12. https://doi.org/10.1007/s42765-019-00024-9.

38. Tomotika, S. (1935). On the instability of a cylindrical thread of a viscous liquid surrounded by another viscous fluid. Proc. Roy. Soc. Lond. A *150*, 322–337. https://doi.org/10.1098/rspa.1935.0104.

39. Kinoshita, C., Teng, H., and Masutani, S. (1994). A study of the instability of liquid jets and comparison with Tomotika's analysis. Int. J. Multiphas. Flow *20*, 523–533. https://doi.org/10.1016/0301-9322(94)90024-4.

40. Du, M., Ye, S., Tang, J., Lv, S., Chen, J., Orava, J., Tao, G., Lan, P., Hao, J., Yang, Z., et al. (2018). Scalable in-fiber manufacture of functional composite particles. ACS Nano *12*, 11130–11138. https://doi.org/10.1021/acsnano.8b05560.

41. Khanarian, G., and Celanese, H. (2001). Optical properties of cyclic olefin copolymers. Opt. Eng. *40*, 1024–1029. https://doi.org/10.1117/1.1369411.

42. Zou, Y., Liu, C., Ren, Z., Zhang, Y., Liu, Z., Xu, Y., Hou, C., Yang, L., Liang, S., and Tao, G. (2022). Flexible and robust low-loss selenium-based multimaterial infrared fibers towards CO2 laser ablation. iScience *25*, 105167. https://doi.org/10.1016/j.isci.2022.105167.

43. Loke, G., Alain, J., Yan, W., Khudiyev, T., Noel, G., Yuan, R., Missakian, A., and Fink, Y. (2020). Computing fabrics. Matter *2*, 786–788. https://doi.org/10.1016/j.matt.2020.03.007.

44. Zou, Y., Ren, Z., Xiang, Y., Liu, C., Gao, A., Huang, S., Yang, L., Hou, C., Guo, H., Yang, G.-Z., and Tao, G. (2024). Flexible fiberbotic laser scalpels: Material and fabrication challenges. Matter *7*, 758–771. https://doi.org/10.1016/j.matt.2024.01.007.

45. Li, P., Wang, Y., He, X., Cui, Y., Ouyang, J., Ouyang, J., He, Z., Hu, J., Liu, X., Wei, H., et al. (2024). Wearable and interactive multicolored photochromic fiber display. Light Sci. Appl. *13*, 48. https://doi.org/10.1038/s41377-024-01383-8.

46. Hu, X., Lu, X., and Qu, J. (2024). Revolutionizing wearable displays with photochromic fibers: Shining as you smile. Matter *7*, 749–751. https://doi.org/10.1016/j.matt.2024.01.032.

47. Tang, C., Yang, Y., Sun, X., and Peng, H. (2023). Scalable production of stretchable conductive fibers for textile electronics. Matter *6*, 1675–1677. https://doi.org/10.1016/j.matt.2023.04.005.

48. Shikha, S., Zheng, X., and Zhang, Y. (2018). Upconversion Nanoparticles-Encoded Hydrogel Microbeads-Based Multiplexed Protein Detection. Nano-Micro Lett. *10*, 31. https://doi.org/10.1007/s40820-017-0184-y.

49. Fulari, A.V., Thanh Duong, N., Anh Nguyen, D., Jo, Y., Cho, S., Young Kim, D., Shrestha, N.K., Kim, H., and Im, H. (2022). Achieving direct electrophoretically deposited highly stable polymer induced CsPbBr3 colloidal nanocrystal films for high-performance optoelectronics. Chem. Eng. J. *433*, 133809. https://doi.org/10.1016/j.cej.2021.133809.

50. Yang, W., Fei, L., Gao, F., Liu, W., Xu, H., Yang, L., and Liu, Y. (2020). Thermal polymerization synthesis of CsPbBr3 perovskite-quantum-dots@copolymer composite: Towards long-term stability and optical phosphor application. Chem. Eng. J. *387*, 124180. https://doi.org/10.1016/j.cej.2020.124180.

51. Liao, H., Guo, S., Cao, S., Wang, L., Gao, F., Yang, Z., Zheng, J., and Yang, W. (2018). A General Strategy for In Situ Growth of All-Inorganic CsPbX3 (X = Br, I, and Cl) Perovskite Nanocrystals in Polymer Fibers toward Significantly Enhanced Water/Thermal Stabilities. Adv. Opt. Mater. *6*, 1800346. https://doi.org/10.1002/adom.201800346.

52. Wang, Z., Fu, R., Li, F., Xie, H., He, P., Sha, Q., Tang, Z., Wang, N., and Zhong, H. (2021). One-Step Polymeric Melt Encapsulation Method to Prepare CsPbBr3 Perovskite Quantum Dots/Polymethyl Methacrylate Composite with High Performance. Adv. Funct. Mater. *31*, 2010009. https://doi.org/10.1002/adfm.202010009.

STAR★METHODS

KEY RESOURCES TABLE

REAGENT or RESOURCE	SOURCE	IDENTIFIER
Chemicals, peptides, and recombinant proteins		
Cyclohexane	Sigma—Aldrich	CAS: 110-82-7
Ferroferric oxide (Fe_3O_4)	Aladdin	CAS: 1309-37-1
N, N-Dimethylacetamide (DMAC)	Sigma—Aldrich	CAS: 127-19-5
Copolymers of cycloolefin (COC)	Zeon	TOPAS® 8007s-04
Polysulfone (PSU)	Solvay	UDEL® P-1700
Software and algorithms		
ImageMeasure	SICHANGYUE Optical Instrument	www.sh-opt.com/
Image J	National Institutes of Health (NIH)	imagej.nih.gov/ij/
Diffrac.EVA	Bruker	www.bruker.com
Fluoracle	Edinburgh Instrument Ltd.	www.edinst.com
LAS AF	Leica	www.leica-microsystems.com

RESOURCE AVAILABILITY

Lead contact

Further information and requests for resources and reagents should be directed to and will be fulfilled by the lead contact, Xvsheng Qiao (qiaoxus@zju.edu.cn)

Materials availability

This study did not generate new unique reagents.

Data and code availability

- All data reported in this paper will be shared by the lead contact upon request.
- This article does not report original code.
- Any additional information required to reanalyze the data reported in this article is available from the lead contact on request.

EXPERIMENTAL MODEL AND STUDY PARTICIPANT DETAILS

This study does not use experimental methods typical in the life sciences.

METHOD DETAILS

COC/PSU preform fabrication

(i) The pellets (millimeter-sized, 8007, Zeon Corporation, Japan) were purchased to the obtain a cylindrical rod of COC with diameter ~2 mm and length ~60 mm by thermally pressing them at 240°C using a customized mold between the thermos-compressor. (ii) Purchased PSU (P-1700, Solvay, USA) pellets were placed into a mold measuring 70 mm in length, 27 mm in width, and 27 mm in height, then they were transformed into a cuboid rod by using the hot press at 290°C. Next, the cuboid PSU rod was processed into a round rod (diameter ~25 mm, Length ~70 mm) through a table-top lathe. Several parallel straight holes slightly larger than COC cylinders were drilled in the PSU section by using a bench top drill. (iii) Inserted the COC rods into the PSU holes for a monolithic preform. Then, the core/cladding structured preform was consolidated at 200°C for 1h in a vacuum oven.

CsPbBr₃ preform fabrication with fluorescent function

(i) The cyclohexane solution (Sigma—Aldrich) has been used to dissolve the COC pellets and stirring was done for 1h (600 rpm, 70°C) to obtain pure and transparent COC/cyclohexane solution. (ii) Then, the $CsPbBr_3$ phosphors with doping ratios ranging from 1%–10% were mixed into the above solution and stirred at 600 rpm for 12 h. (iii) To completely dry the compound the evaporation has been in a vacuum furnace. (iv) Then, the compound was thermally pressed at 240°C through a customized mold between the thermos-compressor to form cylindrical rods with diameter ~2 mm and length ~60 mm. Then, these rods were inserted into the PSU tube for a fluorescent preform.

Janus structured preform fabrication with fluorescent-magnetic multifunction

(i) Both the fluorescent and magnetic composites were fabricated by the dispersion of the functional particles in COC matrix through chemical solution. (ii) Two half-cylindrical rods were machined separately using another customized mold with a diameter ~2 mm and length ~60 mm by using two kinds of composites. Then, they were thermally combined into a round rod. (iii) The round rod was inserted into the PSU tube for a fluorescent-magnetic Janus preform.

Fiber thermal drawing

To provide the suitable pull when the bottom of the preform is just starting to soften, a 2 mm diameter hole was drilled horizontally at 5 mm from the bottom of the preform. A stainless-steel wire with 10g weights was passed through the bottom hole. Then, the assemblies formed were fitted to the custom thermal drawing tower, and the preform was thermally drawn into fibers at 260°C. The preform feeding speed was set and maintained at 1 mm/min, the drawing speed was set around 1.5 m/min. To ensure the uniform diameter of fiber with the diameter 600 ± 10 μm the drawing speed was monitored and controlled accordingly.

Particles fabrication through the PRI method

The core/cladding structured fiber was cut into 20 cm long pieces and subsequently fixed on customized glass sheets with length ~20 cm and width ~2.5 cm with a high temperature tape. Next, these glass sheets were placed in a tube furnace and heat treated at 380°C for 5min. The continuous heat input caused the fibers to soften again and provided the driving force for the core to break into particles by PRI.

Particle release

The PSU cladding has been dissolved with 99.0% DMAC (Sigma—Aldrich) at 100°C for 30–40 min, to release the particles. The washed sample was centrifuged at 15000 rpm for 5min, then the supernatant was removed. After adding DMAC again, the ultrasound was performed for 5min to further dissolve the PSU cladding. This process was repeated five to six times until all the PSU has been removed and the solvent was evaporated, leaving the COC particles on the substrate.

Characterization

Images of the fibers were collected by an optical microscope (OM, CX40M, China) in transmitted light mode. The morphology of particles and the cross-sectional images of the fiber were studied by using a scanning electron microscope (SEM, Zeiss Gemini SEM 360, Germany), and the acceleration voltage was 5 kV. Elemental compositions and distribution of the fiber and the doped material were analyzed via energy dispersive X-ray spectrometer (EDS), during the test, the acceleration voltage was set to 15 kV and the working distance was 8.5 mm. The fluorescence images of $CsPbBr_3$ in the COC microspheres were captured using a confocal laser scanning microscope (CLSM, Leica TCS SP5 II, Germany) by exciting at 405 nm. The vibrating sample magnetometer (VSM, Lakeshore 7404, USA) was used for room temperature magnetic analysis with a field up to 2.0 T, while the pole head diameter was 5cm, the pole pitch was 16.2 mm, the sensitivity was 5×10^{-7} emu, and the measurement ranged from 5×10^{-7} emu–10^3 emu. X-ray diffraction spectra of Fe_3O_4 nanoparticles, $CsPbBr_3$ powder, and composite microspheres were obtained with the X-ray diffractometer (XRD, Bruker D8 Advance, Germany) equipped with Cu Ka radiation, and the measured angle ranged from 10° to 80°, the scan speed was 0.14°/s. Photoluminescence emission spectra and decay curves were recorded on an FLSP920 spectrometer (Edinburgh Instrument Ltd., Livingston, UK) with a 405nm EPLED laser. In this process, the fluorescence lifetime monitoring wavelengths of fluorescent microspheres and perovskite samples were 515nm and 520nm, respectively. Optical absorption spectra have been observed by using the ultraviolet-visible-near infrared spectrophotometer (Shimadzu, UV-4100, Japan). The measurement ranged from 700 nm to 250 nm, and the scan speed was 300 nm/min.

QUANTIFICATION AND STATISTICAL ANALYSIS

Data were expressed as mean $\pm$ SEM (standard error of mean).